Thermally induced sintering and redispersion of Au nanoparticles supported by $Ce_{1-x}Eu_xO_2$ nanocubes and its influence on catalytic activity in CO oxidation

O.S. Bezkrovnyi*[1], P. Kraszkiewicz[1], I. Krivtsov[2,3],
and L. Kepinski[1]

[1.] W. Trzebiatowski Institute of Low Temperature and Structure Research Polish Academy of Sciences, Wroclaw, Poland

[2.] Department of Chemical and Environmental Engineering, University of Oviedo, 33006 Oviedo, Spain

[3] Education and Research Center for Nanotechnology, South Ural State University, Chelyabinsk, Russian Federation

* corresponding author: O.Bezkrovnyi@int.pan.wroc.pl

Abstract

Thermally induced sintering and redispersion of Au nanoparticles supported on $Ce_{1-x}Eu_xO_2$ nanocubes have been investigated. The decisive role of Eu doping in the restriction of thermally induced redispersion of Au nanoparticles supported by $Ce_{1-x}Eu_xO_2$ nanocubes has been established and discussed. The effect of pre-treatment temperature on surface cleaning of $Au/Ce_{1-x}Eu_xO_{2-y}$ catalysts from –OH, $-CO_3$ and NO_3 groups, likely sources of distortion in CO-oxidation tests, has been studied in-situ. Furthermore, we have also explored the effect of Eu doping of ceria support on the number of cationic forms of supported gold nanoparticles. The key role of gold nanoparticle redispersion on active Ce-O-Au sites formation and appropriate - activity in CO-oxidation have shown.

Introduction

CeO_2 is a well-known "active support" for catalytically active gold nanoparticles. The reason for this is its ability to supply oxygen to the metal nanoparticle (e.g., Au) to form active sites [1]. The efficiency of this process depends on oxygen diffusion over the ceria surface, which is facilitated by the presence of oxygen vacancies. There are two main ways of increasing the concentration of oxygen vacancies at the ceria surface. The first one is to obtain ceria nanocrystals shaped as nanocubes terminated by highly active (100) planes, since the energy of oxygen vacancy formation is surface sensitive and follows the sequence {110} <{100} < {111} [2]. Another way is the ceria doping with aliovalent ions [3]. Substitution of two trivalent rare-earth ions for two Ce^{4+} ions in the ceria lattice creates one oxygen vacancy for maintaining electrostatic charge neutrality.

Several factors are determining the activity of Au/ceria catalysts in Red-Ox steps of catalytic reactions such as CO oxidation and the water-gas shift. At first, gold atoms at the periphery of the gold nanoparticles deposited on the support play the primary role as active centers [4,5]. Therefore, high dispersion of metal is required, and any sintering of Au during the reaction will decrease decline~~of~~ its catalytic activity. Fortunately, some examples of the reverse process have been reported. Adibi et al. observed thermally induced redispersion of Pt nanoparticles on Al_2O_3 support, resulting in the bimodal size distribution of Pt nanoparticles: ~2 and <1 nm in size. The small particles are formed by the redispersion, which is driven by Ostwald ripening mass transport via surface diffusion [6]. Therefore, a proper thermal treatment of Au/ceria catalyst could also increase its catalytic activity due to the formation of small (<1 nm) nanoclusters as a result of the redispersion process.

It should be expected that the efficiency of both processes (sintering and redispersion) is strongly sensitive to the concentration of oxygen vacancies at

the surface of ceria support. Ta et al. showed that Au nanoparticles are firmly fixed on ceria support through intimate contact with the surface oxygen vacancies [5]. As discussed above, the number of oxygen vacancies at the surface of ceria nanoparticles directly depends on the concentration of aliovalent dopant ions (e.g., Eu^{3+}). Thus, Eu^{3+} incorporation into the crystal lattice of ceria support should have a significant impact on the thermally induced sintering/redispersion processes of Au nanoparticles. Though such effect can significantly affect the total catalytic activity of Au/ceria systems, it remains unexplored until now [7].

The second factor, responsible for the high efficiency of the Au/ceria system in the CO-oxidation process is charging of gold nanoparticles. DFT calculation revealed some electronic charge transfer from Au to the support at the Au-ceria interface, leading to oxidation of Au and reduction of ceria support [8]. Moreover, Guo et al. demonstrated that single Au atoms on ceria support are fully oxidized, gold clusters smaller than 2 nm have mixed cationic and metallic states, while 3-4 nm particles are metallic Au structures [9]. Thus, thermally induced sintering/redispersion processes should have a significant impact on Au nanoparticles charging, which is a crucial step in CO-oxidation reaction. Despite a large number of publications devoted to Au/CeO_2, information about $Au/Ce_{1-x}Ln_xO_{2-y}$ (Ln – trivalent lanthanide) systems is scarce.

The present study aims to determine the effect of Eu doping on the thermally induced sintering and redispersion of Au nanoparticles on ceria nanocubes and on charging of Au nanoparticles. The influence of these processes on the catalytic activity of the $Au/Ce_{1-x}Eu_xO_{2-y}$ nanoparticles in the CO oxidation was also investigated and discussed.

Experimental part

Cube-shaped nanocrystals of ceria were synthesized by microwave-assisted hydrothermal method (MAHT), described in more detail in our previous works

[10,11]. In short, $Ce(NO_3)_3 \cdot 6H_2O$ and $Eu(NO_3)_3 \cdot 5H_2O$ first dissolved in distilled water. Next, the obtained solution was mixed with an appropriate amount of aqueous NaOH solution and then stirred for 60 min. The final solution was treated at 200°C for 3 h under autogenous pressure in an autoclave. The obtained precipitate powder was washed and dried at 60ºC for 12 h.

Au nanoparticles were deposited on the ceria nanocubes using a deposition-precipitation method similar to that used by Lin et al. [12]. 100 mg of ceria nanocubes, 4 mg $HAuCl_4$, 256 mg $(NH_2)_2CO$ and 12 ml H_2O were mixed to form a suspension. The suspension was stirred and kept at 80°C in a silicone oil bath for 24 h. Au/ceria particles were washed and dried at 50°C for 12 h. The as-prepared particles were annealed in air at 300°C for 2 h.

Crystal structure of the samples was determined by powder X-ray diffraction (XRD) using X'Pert PRO PANalytical diffractometer with CuKα radiation. X'Pert High-Score Plus program was used for display and analysis of the diffraction patterns by Rietveld method. Chemical composition and element distribution in the samples were checked with FEI NovaNanoSEM 230 and JEM-F200 STEM microscopes equipped with Energy Dispersive Spectrometers (EDS).

The morphology of the particles was determined by transmission electron microscopy (TEM), using a Philips CM-20 SuperTwin instrument operating at 160 kV and FEI Titan (S)TEM operating at 300 kV. The samples for TEM measurements were ultrasonically dispersed in methanol, and a droplet of the suspension was deposited on a copper grid coated with a carbon film.

DRIFT spectroscopy was carried out using a Thermo Nicolet Nexus FT-IR equipped with a Smart Collector Accessory and a MCT/A detector, configured to record with a resolution of 4 cm^{-1} and to collect 60 scans/spectrum. The catalyst sample was placed inside the catalytic chamber where a thermocouple

controlled the temperature, and a synthetic air was purged through the system at 20 ml min^{-1}. Spectra were recorded in the 4000–650 cm^{-1} wavenumber range.

The surface composition and the oxidation state of the atoms in the materials were measured by X-ray photoelectron spectroscopy (XPS), using a SPECS system equipped with a Hemispherical Phoibos analyzer operating at 225 W, 13 kV and 17.5 mA in constant pass energy, using Mg Kα radiation (hν = 1253.6 eV).

H_2-TPR (temperature programmed reduction) was performed by heating the samples with a heating rate of 10°C min^{-1} up to 900°C in H_2 (5 vol.%)/Ar flow. The hydrogen consumption was monitored by a thermal conductivity detector (TCD). Weights of the samples were 50 mg.

The catalytic activity of the samples was tested in CO oxidation. Typically, 50 mg of the catalyst was placed in a quartz microreactor (Autochem II 2920, Micromeritics). The gas stream containing 1% CO, 5% O_2, balanced with He (total flow rate 50 ml/min), was introduced into the reactor at room temperature and the light-off curves were obtained with a temperature ramp rate of 3°C min^{-1}. The outlet gas was analyzed by a mass spectrometer (OmniStar QMS-200, Pfeiffer Vacuum) calibrated with gas mixtures of known composition. All used gases were of high purity (>99.99 %).

Results and discussions.

I) TEM investigations

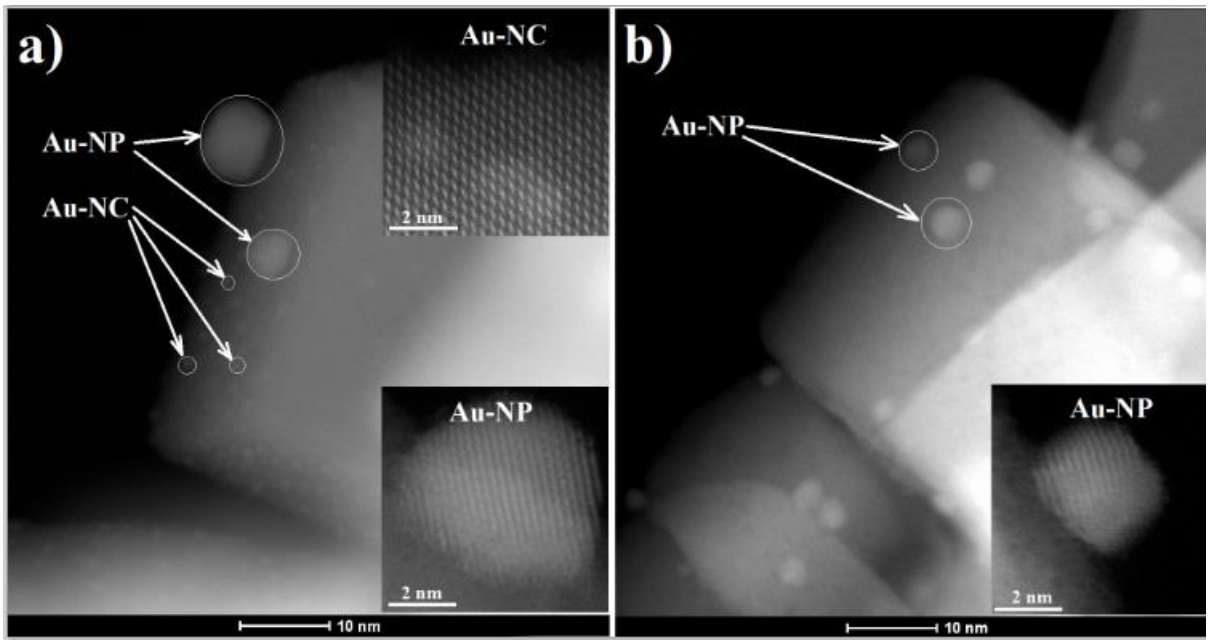

Figure 1. STEM images of Au/CeO_{2-y} (a) and Au/$Ce_{0.70}Eu_{0.30}O_{2-y}$ (b) samples pre-treated at 300°C for 3 h in air. *HR-STEM images of Au nanoparticles (NP) and nanoclusters (NC) are shown as insets.*

In our previous works, we have shown that ceria nanocubes (supports for Au nanoparticles) are single crystals, predominantly terminated by {100} faces, with a small contribution of {110} and {111} faces at the edges and corners, respectively [11;13]. Figure 1 presents overview images of CeO_{2-y} and $Ce_{0.70}Eu_{0.30}O_{2-y}$ nanocubes decorated with gold nanoparticles and pre-treated at 300°C for 3 h in air. The Au nanoparticles (NP) are single crystals, exposing {100} and {111} faces (see insets to Fig. 1b). EDS data show that the actual europium concentrations in the samples agree with the nominal content set by the Eu concentration in the precursor solution and the Au content in all samples is appx. 1at.% (See Electronic Supporting Information Table S1).

Interestingly, Au particles supported on pure CeO_{2-y} have bimodal size distribution. Both nanoclusters (NC) less than 1 nm in size and 3-6 nm

nanoparticles (NP) are present (see Fig. 1-a). On the contrary, Au NP supported on $Ce_{0.70}Eu_{0.30}O_{2-y}$ are more homogeneous having dimensions of 2-4 nm (see Fig. 1-b).

It should be noted that typical sizes of Au nanoparticles on CeO_{2-y} and $Ce_{0.70}Eu_{0.30}O_{2-y}$ nanocubes after deposition (after drying at 60°C) were 2-4 and 1-3 nm (cf. Fig. S1 and Fig.S2).

The differences in the dispersion of Au NP over pure and Eu-doped ceria nanocubes after treatment at 300°C can be explained in the following way. There are two primary mechanisms of the thermally driven growth process of noble metal nanoparticles. In the first (PM), individual particles migrate on the support surface and coalesce with other particles after collision [14, 15]. The second mechanism is Ostwald ripening (OR), where single atoms detach from small particles and diffuse to larger ones, either over the support surface or via the gas phase [15]. Akita et al., [16, 17] show that Au nanoparticles are immobile at the surface of CeO_2 support in the air at temperature up to 600°C, and atomic transport is responsible for the observed particle growth. The authors also noted significantly hindered growth of Au particles in reducing atmosphere in the same temperature range and attributed this to the presence of oxygen vacancies. Thus, in our case (at temperatures up to 300°C) OR should be a dominant process responsible for the sintering of Au nanoparticles on a ceria support. The efficiency of the OR process depends directly on the rate of surface diffusion of gold atoms over ceria support. In turn, there is a reason to believe that the rate of surface diffusion of gold atoms strongly depends on the number of oxygen vacancies on the surface of ceria support. Ta et al., show that Au nanoparticles are firmly fixed through intimate contact with the surface oxygen vacancies on ceria nanorods [5]. We increased the number of oxygen vacancies at the surface of ceria nanoparticles by doping with aliovalent Eu^{3+} ions, so that the doped ceria nanocubes have more anchoring sites for gold nanoparticles than pure CeO_2 nanocubes.

Therefore, the surface diffusion of gold atoms over ceria support decreases with Eu doping. It results in inhibition of the sintering of Au nanoparticles. Typical sizes of Au nanoparticles in the as-prepared Au/CeO_{2-y} and $Au/Ce_{0.70}Eu_{0.30}O_{2-y}$ are 1-3 and 2-4 nm respectively, while after annealing at 300°C they are 5-8 nm and 2-3 nm, respectively (cf. Fig. S2). Moreover, dopant induced anchoring of Au nanoparticles prevents the "redispersion" process responsible for the formation of < 1nm gold nanoclusters on undoped CeO_{2-y}. It has a significant implication on the reducibility and total catalytic activity of Au/ceria system (see more details in chapters "H_2-TPR" and "CO-oxidation").

II) DRIFT investigations

The presence of extraneous groups adsorbed on the catalyst surface has a significant impact (both positive and negative) on catalytic activity (cf. supplementary materials). In order to determine the evolution of species present on the surface of the catalysts during pre-treatment (thermal activation), we examined the $Au/Ce_{1-x}Eu_xO_{2-y}$ (x=0; 0.30) samples using in-situ diffuse reflectance FTIR measurements. Fig. 2 shows the in-situ DRIFT spectra of the Au/CeO_{2-y} sample acquired in the air at various temperatures. Analogous spectra of $Au/Ce_{0.70}Eu_{0.30}O_{2-y}$ sample are presented in the supporting information (cf. Fig. S3).

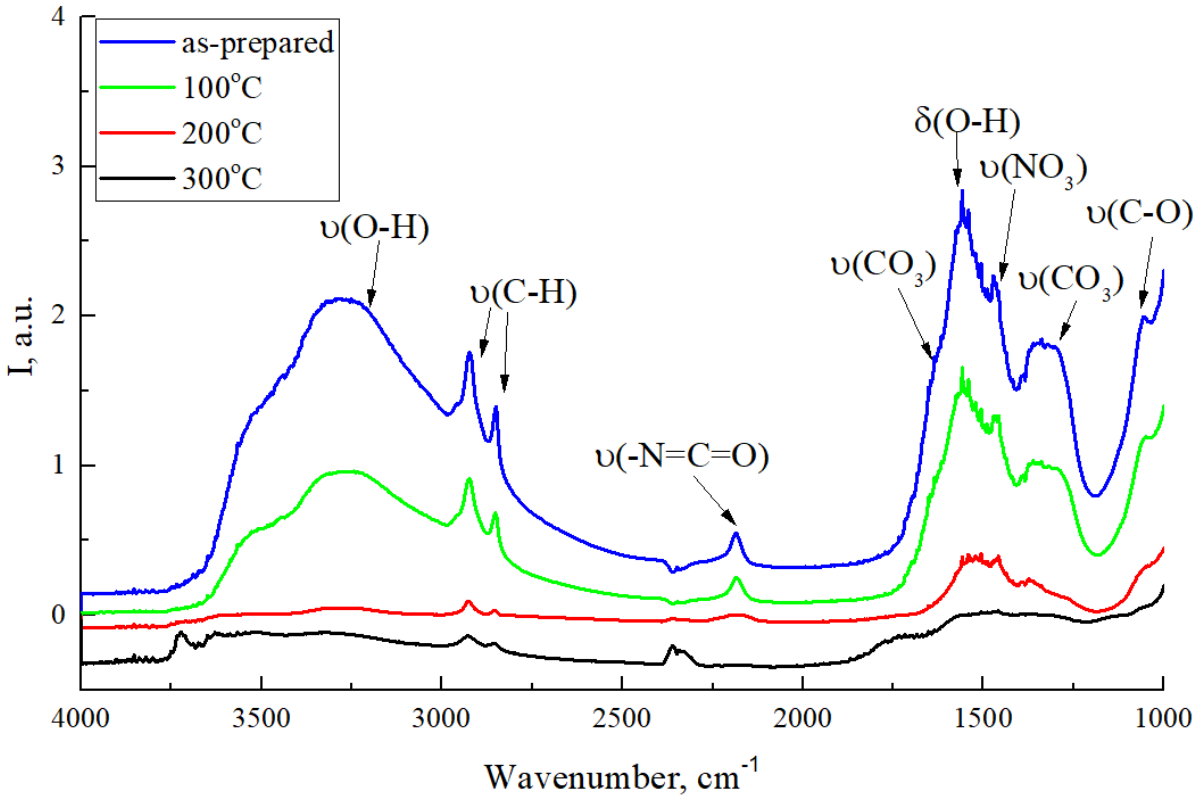

Figure 2. DRIFT spectra of the Au/CeO_{2-y} sample acquired at different temperatures.

DRIFT spectra of the as-prepared samples show the following characteristic features. The broad, intense bands at 3300 and 1570 cm^{-1} correspond to the ν(O–H) mode of (H-bonded) water molecules and δ(OH), respectively [18,19]. The OH vibration bands show a non-negligible shift towards lower wavenumbers with respect to that normally observed for the pure oxide surface (3420 and 1640 cm^{-1}, respectively). The weak bands at 2922 and 2850 cm^{-1} are assigned to the ν(C–H) mode of organic moieties [18; 20]. The low-intensity band at 2182 cm^{-1} can most likely be attributed to ν(-N=C=O) vibrations of isocyanate groups adsorbed on metal (Au) NPs [21]. Two strong bands at 1600 cm^{-1} and 1340 cm^{-1} are attributed to ν(CO_3) vibrations of carbonate groups, whereas the band at 1470 cm^{-1} is attributed to ν(NO_3) vibrations of nitrate

groups [21]. The band at 1058 cm^{-1} may be assigned to the stretching ν(C–O) mode of adsorbed organic mentions [20].

It should be noted that DRIFT spectra of the as-prepared Au/CeO_{2-y} and $Au/Ce_{0.70}Eu_{0.30}O_{2-y}$ samples show some differences (compare Fig. 3 and Fig. S3). For instance, increasing europium content in ceria leads to enhancement in the intensity of hydroxide and especially carbonate related bands. Thus, the main impurities in the as-prepared Au/ceria samples are hydroxyl groups, adsorbed water, carbonates and nitrates.

Annealing in air significantly attenuates the –OH, $-CO_3$, $-NO_3$ and also organic moieties related bands (cf. Fig. 3 and Fig. S3). It appears that annealing at 300°C is enough for almost complete surface cleaning of the $Au/Ce_{1-x}Eu_xO_{2-y}$ catalysts from –OH, $-CO_3$ and NO_3 groups, likely sources of distortions in the CO-oxidation tests.

III) XPS investigations

Surface composition of our samples was investigated by XPS technique. As we mentioned in the introduction the charging of gold nanoparticles plays a critical role in CO oxidation reactions, therefore, we focused on the study of an oxidation state of gold nanoparticles.

The XPS spectra of Au 4f region of the $Au/Ce_{1-x}Eu_xO_{2-y}$ samples are presented on Fig. 3. The spectra comprise three Au $4f_{7/2}$ and Au $4f_{5/2}$ doublets of Au^0, Au^+ and Au^{3+}. The deconvolution of the Au 4f spectra was carried out considering an Au $4f_{7/2}$ Au $4f_{5/2}$ band split of 3.7 eV and using the ratio of 4:3 between the integrated intensities of the Au $4f_{7/2}$ and Au $4f_{5/2}$ contributions.

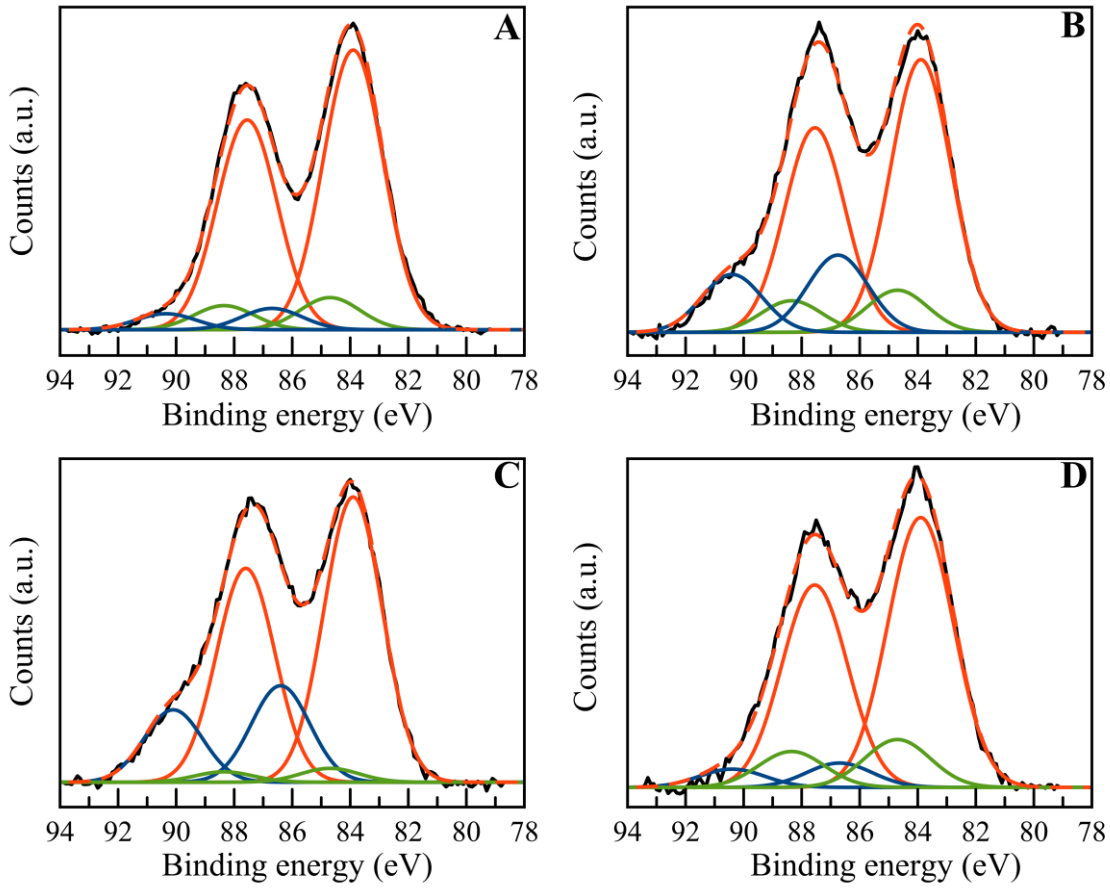

Figure 3. Au 4f regions of XPS spectra for Au/CeO_{2-y}(a), Au/$C_{e0.90}Eu_{0.10}O_{2-y}$(b), Au/$Ce_{0.80}Eu_{0.20}O_{2-y}$ (c), Au/$Ce_{0.70}Eu_{0.30}O_{2-y}$ (d). All samples are pre-treated at 300°C for 3 h in air. Measured spectra (black), their deconvolution into three doublets: Au^0 (red), Au^+ (green) and Au^{3+} (blue) as well as summary (dash red) are shown.

Table 1 presents Au^0 (metallic gold) and $Au^{\delta+}$ ($Au^{\delta+}$ - a cationic form of gold, i.e., Au^+ and Au^{3+}) contents for the samples, calculated by comparison of areas under Au^0, Au^+ and Au^{3+} curves. As seen from Table 1, the $Au^{\delta+}$ content depends in a complicated way on the europium content in ceria support. It first increases up to x=0.10, then starts to decline.

Table 1. Au^0 and $Au^{\delta+}$ content in $Au/Ce_{1-x}Eu_xO_{2-y}$ samples.

Sample	Au^0, %	$Au^{\delta+}$, %
Au/CeO_{2-y}	84	16
$Au/Ce_{0.90}Eu_{0.10}O_{2-y}$	69	31
$Au/Ce_{0.80}Eu_{0.20}O_{2-y}$	72	28
$Au/Ce_{0.70}Eu_{0.30}O_{2-y}$	79	21

To explain the observed dependence, we must consider the morphology of Au phase in the samples. For Au/CeO_2 a bimodal size distribution of Au particles was observed. Both very small (≤1nm) and large (> 5 nm) particles were detected by HAADF method (MEANING OF HAADF?). According to the literature, single Au atoms on ceria nanorods are fully oxidized, gold clusters < 2 nm have mixed cationic and metallic states, while 3-4 nm particles are reduced Au structures [9]. We may expect therefore some content of cationic $Au^{\delta+}$ due to the presence of very small Au structures (atoms or clusters).

In our case, doping with Eu^{3+} increases initially the net positive charge of Au particles, especially Au^{3+} (Table 1), though according to TEM, it decreases the number of the smallest particles (< 1 nm). Explanation of this apparent inconsistency is based on the fact that Au^{3+} contribution mainly comes from individual Au atoms adsorbed at the ceria surface [22], that are invisible in HAADF images. Due to the presence of a large number of surface defects in the Eu doped ceria, the Au atoms are strongly bonded to the surface, and do not aggregate during pretreatment at 300°C, as it happens for pure ceria support. In consequence, they are not detected by HAADF. At the highest Eu content (x = 0.3) there is a net decline in the amount of cationic gold (Table 1). The possible reason is an aggregation of oxygen vacancies, with a simultaneous decrease of the number of single atoms at the surface.

However, presented above explanation of the effect of Eu doping of ceria support on the gold nanoparticles charge is presumptive and needs more experimental confirmation.

IV) H_2-TPR investigations

H_2-TPR profiles of the Au/$Ce_{1-x}Eu_xO_{2-y}$ samples can be divided into two regions: low (< 200°C) and high (600 – 900°C) temperature. High-temperature peak (at 600–900°C) is very similar to that observed for bare $Ce_{1-x}Eu_xO_{2-y}$ (cf. Fig. S4) [11], and shifts smoothly to lower temperatures with increasing europium content. It is thus assigned to a bulk reduction of ceria.

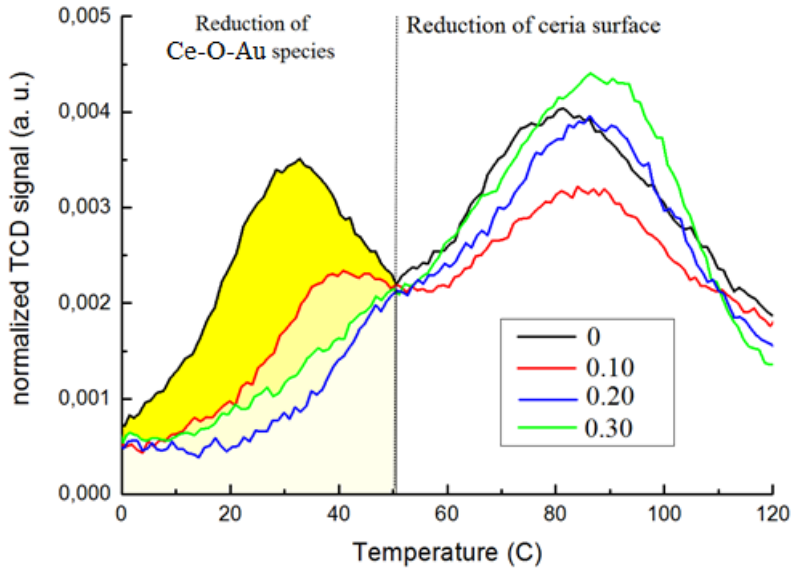

Figure 4. The low-temperature region of H_2-TPR profiles of the Au/$Ce_{1-x}Eu_xO_{2-y}$ catalysts (pre-treated at 300°C for 3 h in air). (IMPROVE THE LEGEND…x=0, 0.1..

Since the easily reducible species at the Au-ceria interface are vital to catalytic performance in oxidizing reactions, we will discuss the low-temperature region of the H_2-TPR profiles in detail (Fig. 4). According to the literature, hydrogen consumption in this region (< 200 °C) of H_2-TPR curve of Au/ceria system is

mainly attributed to the surface reduction of ceria [23-25], but the reduction of oxidized gold species cannot be excluded [26]. In our case, two reduction peaks at ~35 and ~90°C can be distinguished for all samples. Acerbi et al., also reported a double peak structure in this region and stated that the first component could be assigned to the reduction of metal oxide species, while the second component to the surface reduction of ceria [27]. Though Chang et al., reported that the reduction of gold oxides (Au^sO_x) occurs at a much lower temperature of −90°C in Au/Al_2O_3 [28], we assume, in accordance with Concepcion et al., [29], that ceria support stabilizes Au^+ and Au^{3+} forms of gold, so Au-O peak can be shifted to higher temperatures. Moreover, H_2-consumption for 100 mg Au/CeO_{2-y} sample (which has a maximum intensity of the first peak at ~35°C) is ~$2.8\cdot10^{-5}$ mol. However, hypothetic H_2-consumption for 100 mg of Au/CeO_{2-y} (2.7 wt.% Au) with fully oxidized gold (Au_2O_3) is almost three orders of magnitude higher (~$4.2\cdot10^{-2}$ mol). Thus, we attribute the first peak (at ~35°C) to the reduction of Ce^{3+}-O-$Au^{\delta+}$ species on the gold−ceria perimeters. The remaining O-$Au^{\delta+}$ sites in the first layer of atoms at the interface with the support are shielded from the environment and don't have a significant impact on the 35°C peak.

Another issue is the observed decline of the intensity of the first peak with increasing concentration of europium. As we mentioned above (see Fig. 2), thermally activated Au/CeO_{2-y} sample contains Au particles with bimodal size distribution: gold clusters less than 1 nm in size and 5-8 nm nanoparticles. On the contrary, highly Eu-doped $Au/Ce_{1-x}Eu_xO_{2-y}$ materials contain few nanometer-sized gold nanoparticles and individual Au atoms. We assume that the reduction of Ce^{3+}-O-$Au^{\delta+}$ species on small (<0.5 nm) gold clusters makes the main contribution to the first peak (at 35°C). Taking into account that doping of ceria support with Eu inhibits the formation of Au sub-nanometer clusters (see Fig 2), the lowering of Ce^{3+}-O-$Au^{\delta+}$ related peak with increasing of the Eu-doping level becomes clear.

The second peak (at 90°C) does not change noticeably with Eu doping. We attribute this peak to the surface reduction of ceria support, facilitated by the presence of Au particles, which activate hydrogen molecules [23-25].

V) CO-oxidation tests

CO-oxidation light-off curves were measured for Au/Ce1-xEuxO2-y samples (x = 0; 0.10; 0.20; 0.30) to evaluate the effect of Eu doping of ceria nanocubes on the catalytic activity of the supported Au particles (Fig. 5).

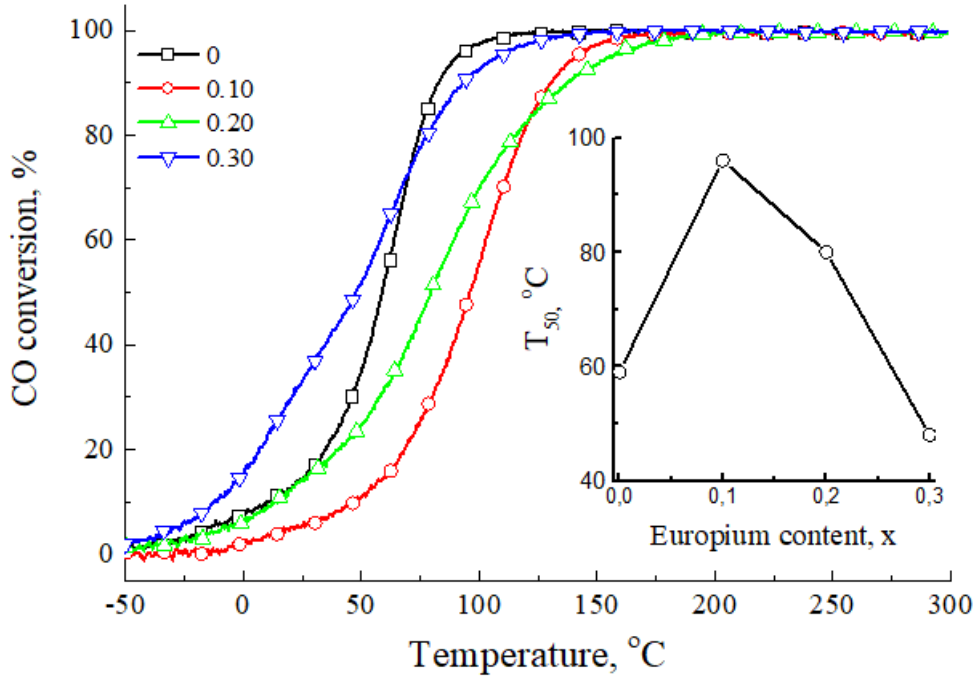

Figure 5. CO oxidation light-off curves for the $Au/Ce_{1-x}Eu_xO_{2-y}$ samples, where x=0; 0.10; 0.20; 0,30. On the insert – dependence of T_{50} on the Eu content in ceria support.

The dependence of the catalytic activity (defined as a temperature of half-conversion T_{50}) of the $Au/Ce_{1-x}Eu_xO_{2-y}$ samples on the europium content has two regions. Initially, an increase of the europium content in ceria support from x=0

up x=0.10 results in the decrease of the catalytic activity (T_{50} increases from 60 to 95°C). Then, the increase of the europium content up to x=0.30 diminishes the catalytic activity (T_{50} decreases from 95 to 47°C).

This observation agrees well with XPS data, and with the literature [30], showing that neutral (Au^0) in Au nanoparticles, but not ionic Au^{3+}, is mainly responsible for the activity in low-temperature CO oxidation.

It is known, that doping ceria with trivalent ions increases the concentration of oxygen vacancies and, as a consequence, enhances the oxygen mobility, which is crucial for high activity in CO oxidation [31]. Hernández et al., [32] studied the activity of Au/CeO_2 and $Au/Ce_{0.9}Eu_{0.1}O_{2-\delta}$ catalyst in CO oxidation and observed that Eu-doped catalyst was less active (T_{50} = 134 and 185°C, respectively; catalysts activated at 300°C in air). The result was somehow unexpected, because, in other work they showed, that doping ceria with 10 at% of europium enhances its activity in CO oxidation [31]. Raman spectroscopy showed that deposition of gold on the Eu doped ceria caused the signal from oxygen vacancies to vanish due to filling oxygen vacancies by gold [32]. Unfortunately, they did not study catalysts with a higher concentration of Eu. As can be seen from our results, the higher concentration of Eu (x=0.20-0.30) enhanced catalysts activity. To explain this, the electronic structure of Au must be considered. According to XPS, the activity of the catalysts correlates quite well with the concentration of cationic gold species, i.e., the least active sample contains the highest concentration of cationic Au. In the literature, there is no consensus which state of gold is active in CO oxidation. Some authors assigned the high activity of gold catalysts to the high concentration of cationic Au [29,33,34]. Other authors reported that cationic gold is not active in the low-temperature CO oxidation, and the metallic gold is the active one [35,36]. Our results show that there is no direct positive correlation between the content of cationic gold species and the activity in CO oxidation.

Ta et al., proposed that Au atoms at the gold−ceria periphery are the active sites for the reaction of adsorbed CO molecules with active oxygen species on ceria to form CO_2 molecules [5]. Thus, we attribute the initial decline of the catalytic activity to the decreased population of small (≤1nm) Au nanoclusters on Eu-doped ceria support (See Fig. 2). This hypothesis consents with H_2-TPR data (See Fig. 4) – the intensity of Ce^{3+}-O-$Au^{\delta+}$ peak decreases with the increase of the europium content in ceria support.

It can be attributed to the preferential formation of active Ce-O-Au sites due to the high number of Eu-induced oxygen vacancies at the surface of ceria support. This supposition agrees with Reddy et al., [37], who state that oxygen vacancies act as active sites for the dissociation of gaseous oxygen. Thus, doping of ceria with Ln^{3+} facilitates the reduction of ceria and increases the oxygen storage/release capacity 4-5 times compared to pure ceria [37]. Our previous results are also in good agreement with their data because we demonstrated that the doping of ceria nanocubes with Eu^{3+} increased their reducibility [11].

Conclusions

The effect of Eu doping on thermal stability of Au nanoparticles on ceria nanocubes was investigated by HR-STEM technique. It was shown that pre-treatment of Au nanoparticles supported by pure CeO_{2-y} at 300°C results in extensive Au particle growth via the Ostwald ripening mechanism. As a result, a bimodal particle size distribution occurs having two different sizes: ≤1 nm and 3-6 nm. Doping of ceria support with Eu leads to the anchoring of Au nanoparticles. It prevents the "redispersion" process responsible for < 1nm gold nanoclusters formation. The effect of pre-treatment temperature on the desorption of extraneous groups adsorbed on Au/$Ce_{1-x}Eu_xO_{2-y}$ catalyst surface was investigated by in-situ DRIFT technique. It was shown that the pre-treatment at 300°C is enough for almost complete surface cleaning of all the

$Au/Ce_{1-x}Eu_xO_{2-y}$ catalysts from –OH, $-CO_3$ and NO_3 groups, -likely sources of distortion in CO-oxidation tests. The valency of gold nanoparticles supported on $Ce_{1-x}Eu_xO_{2-y}$ nanocubes was examined by XPS. It was shown that Eu doping of ceria support decreases the contribution of $Au^{\delta+}$ forms of gold. The key role of gold nanoparticle redispersion on the formation of active Ce-O-Au sites and in consequence on the activity in CO-oxidation was shown by H_2-TPR and catalytic tests in CO-oxidation reaction.

Acknowledgements

The authors thank Silesian Association of Electron Microscopy and Wrocław Research Centre EIT+, Wroclaw, Poland for access to the Titan microscope and Dr. W. Mista for help with CO – oxidation tests. This work was financially supported by NCN (UMO-2017/27/N/ST5/02731) and Spanish MINECO (MAT2016-78155-C2-1-R and CTQ2014-52956-C3-1-R).

References

1. M.M. Schubert, S. Hackenberg, A.C. van Veen, M. Muhler, V. Plzak, R.J. Behm, CO Oxidation over Supported Gold Catalysts—"Inert" and "Active" Support Materials and Their Role for the Oxygen Supply during Reaction, J. Catal. 197 (2001) 113-122
2. J.C. Conesa, Computer modeling of surfaces and defects on cerium dioxide, Surface Science 339 (1995) 337-352
3. N. Shehata, K. Meehan, M. Hudait and N. Jain, J. Nanopart. Res., 2012, 14, 1173
4. T. Fujitani and I. Nakamura, Mechanism and Active Sites of the Oxidation of CO over Au/TiO_2, Angew. Chem. Int. Ed., 2011, 50, 10144 –10147
5. N. Ta, J. Liu, S. Chenna, P.A. Crozier, Y. Li, A. Chen and W. Shen, Stabilized Gold Nanoparticles on Ceria Nanorods by Strong Interfacial Anchoring, J. Am. Chem. Soc., 2012
6. Pooya Tabib Zadeh Adibi, Torben Pingel, Eva Olsson, Henrik Gronbeck, and Christoph Langhammer, Pt Nanoparticle Sintering and Redispersion on a Heterogeneous Nanostructured Support, J. Phys. Chem. C 2016, 120, 14918−14925

7. Willinton Y. Hernandez, Francisca Romero-Sarria, Miguel A. Centeno, and Jose A. Odriozola, J. Phys. Chem. C 2010, 114, 10857–10865
8. Zhang et ell., J. Am. Chem. Soc., 132, (2010), 2175–2182
9. Li-Wen Guo, Pei-Pei Du, Xin-Pu Fu, Chao Ma, Jie Zeng, Rui Si, Yu-Ying Huang, Chun-Jiang Jia, Ya-Wen Zhang and Chun-Hua Yan, Contributions of distinct gold species to catalytic reactivity for carbon monoxide oxidation, Nature Communications volume 7, Article number: 13481 (2016)
10. O.S. Bezkrovnyi, R. Lisiecki, L. Kepinski, Relationship between morphology and structure of shape-controlled CeO_2 nanocrystals synthesized by microwave assisted hydrothermal method, Cryst. Res. Technol. 51 (2016) 554–560
11. Oleksii Bezkrovnyi, Małgorzata A. Małecka, Radoslaw Lisiecki, Volodymyr Ostroushko, Andrew G. Thomas, Sandeep Gorantla and Leszek Kepinski, The effect of Eu doping on the growth, structure and red-ox activity of ceria nanocubes, CrystEngComm, 2018, 20, 1698–1704
12. Yuyuan Lin, Zili Wu, Jianguo Wen, Kunlun Ding, Xiaoyun Yang, Kenneth R. Poeppelmeier, and Laurence D. Marks, Adhesion and Atomic Structures of Gold on Ceria Nanostructures: The Role of Surface Structure and Oxidation State of Ceria Supports, Nano Lett. 2015, 15, 5375−5381
13. O.S. Bezkrovnyi, P. Kraszkiewicz, M. Ptak and L. Kepinski, Thermally induced reconstruction of ceria nanocubes into zigzag {111}-nanofacetted structures and its influence on catalytic activity in CO oxidation, Catalysis Communications 117 (2018) 94–98
14. E. Ruckenstein, B. Pulvermacher, Kinetics of Crystallite Sintering During Heat Treatment of Supported Metal Catalysts, AIChE J., 1973, 19, 356 – 364
15. F. Behafarid, B.R. Cuenya, Towards the Understanding of Sintering Phenomena at the Nanoscale: Geometric and Environmental Effects, Top Catal., 2013, 56, 1542–1559
16. T. Akita, K. Tanaka, M. Kohyama, TEM and HAADF-STEM study of the structure of Au nano-particles on CeO2, J Mater Sci (2008) 43:3917–3922.
17. T. Akita, K. Tanaka, M. Kohyama, M. Haruta, Analytical TEM study on structural changes of Au particles on cerium oxide using a heating holder, Catalysis Today 122 (2007) 233–238

18. Mirosław Zawadzki, Preparation and characterization of ceria nanoparticles by microwave-assisted solvothermal process, Journal of Alloys and Compounds 454 (2008) 347–351

19. Dolly Valechha, Suchita Lokhande, Mariana Klementova, Jan Subrt, Sadhana Rayalu and Nitin Labhsetwar, Study of nano-structured ceria for catalytic CO oxidation, J J. Mater. Chem., 2011, 21, 3718–3725

20. Kamal M.S. Khalil, Leena A. Elkabee, Brian Murphy, Preparation and characterization of thermally stable porous ceria aggregates formed via a sol–gel process of ultrasonically dispersed cerium(IV) isopropoxide, Microporous and Mesoporous Materials 78 (2005) 83–89

21. V. Matsouka, M. Konsolakis, R.M. Lambert, I.V. Yentekakis, In situ DRIFTS study of the effect of structure (CeO2–La2O3) and surface (Na) modifiers on the catalytic and surface behaviour of Pt/γ-Al2O3 catalyst under simulated exhaust conditions, Applied Catalysis B: Environmental 84 (2008) 715–722

22. J. H. Carter, X. Liu, Q. He, S. Althahban, E. Nowicka, S. J. Freakley, L. Niu, D. J. Morgan, Y. Li, J. W. H. Niemantsverdriet, S. Golunski, C. J. Kiely, and G. J. Hutchings, Activation and Deactivation of Gold/Ceria–Zirconia in the Low-Temperature Water–Gas Shift Reaction, Angew. Chem. Int. Ed. 2017, 56, 16037 –16041

23. Xiao-Ying Wang, Shu-Ping Wang, Shu-Rong Wang, Ying-Qiang Zhao, Jing Huang, Shou-Min Zhang, Wei-Ping Huang, and Shi-Hua Wu, The preparation of Au/CeO2 catalysts and their activities for low-temperature CO oxidation, Catalysis Letters, 2006, Vol. 112, 115-119

24. Qi Fu, Adam Weber and Maria Flytzani-Stephanopoulos, Nanostructured Au–CeO2 catalysts for low-temperature water–gas shift, Catalysis Letters Vol. 77, No. 1–3, 2001

25. Yanjie Zhang, Yanyan Zhao, Han Zhang, Liyuan Zhang, Huipeng Ma, Peipei Dong, Desheng Li, Jingjie Yu and Guanying Cao, Investigation of oxygen vacancies on Pt- or Au modified CeO2 materials for CO oxidation, RSC Adv., 2016, 6, 70653–70659

26. Q. Fu, S. Kudriavtseva, H. Saltsburg, M. Flytzani-Stephanopoulos, Gold–ceria catalysts for low-temperature water-gas shift reaction, Chem. Eng. J. 93 (2003) 41–53

27. Nadia Acerbi, Shik Chi Tsang, Stan Golunski and Paul Collier, A practical demonstration of electronic promotion in the reduction of ceria coated PGM catalysts, Chem. Commun., 2008, 1578–1580

28. Chao-Kang Chang, Yeong-Jey Chen, Chuin-tih Yeh, Characterizations of alumina-supported gold with temperature-programmed reduction, Applied Catalysis A: General 174 (1998) 13-23

29. Patricia Concepcion, Silvio Carrettin, Avelino Corma, Stabilization of cationic gold species on Au/CeO2 catalysts under working conditions, Applied Catalysis A: General 307 (2006) 42–45\

30. L.W. Guo, P.P. Du, X.P. Fu, C. Ma, J. Zeng, R. Si, Y.Y. Huang, C.J. Jia, Y.W. Zhang, C.H. Yan, Contributions of distinct gold species to catalytic reactivity for carbon monoxide oxidation, Nat. Commun. 7 (2016) 13481. doi:10.1038/ncomms1348

31. W.Y. Hernández, M.A. Centeno, F. Romero-Sarria, J.A. Odriozola, Synthesis and Characterization of Ce1−xEuxO2−x/2 Mixed Oxides and Their Catalytic Activities for CO Oxidation, J. Phys. Chem. C. 113 (2009) 5629–5635. doi:10.1021/jp8092989

32. W.Y. Hernández, F. Romero-Sarria, M.A. Centeno, J.A. Odriozola, In Situ Characterization of the Dynamic Gold−Support Interaction over Ceria Modified Eu3+. Influence of the Oxygen Vacancies on the CO Oxidation Reaction, J. Phys. Chem. C. 114 (2010) 10857–10865. doi:10.1021/jp1013225

33. J. Guzman, B.C. Gates, Catalysis by Supported Gold: Correlation between Catalytic Activity for CO Oxidation and Oxidation States of Gold, J. Am. Chem. Soc. 126 (2004) 2672–2673. doi:10.1021/ja039426e

34. G.J. Hutchings, M.S. Hall, A.F. Carley, P. Landon, B.E. Solsona, C.J. Kiely, A. Herzing, M. Makkee, J.A. Moulijn, A. Overweg, J.C. Fierro-Gonzalez, J. Guzman, B.C. Gates, Role of gold cations in the oxidation of carbon monoxide catalyzed by iron oxide-supported gold, J. Catal. 242 (2006) 71–81. doi:10.1016/j.jcat.2006.06.001

35. L. Delannoy, N. Weiher, N. Tsapatsaris, A.M. Beesley, L. Nchari, S.L.M. Schroeder, C. Louis, Reducibility of supported gold (III) precursors: influence of the metal oxide support and consequences for CO oxidation activity, Top. Catal. 44 (2007) 263–273. doi:10.1007/s11244-007-0299-3;
30

36. S. Wei, X.-P. Fu, W.-W. Wang, Z. Jin, Q.-S. Song, C.-J. Jia, Au/TiO2 Catalysts for CO Oxidation: Effect of Gold State to Reactivity, J. Phys. Chem. C. 122 (2018) 4928–4936. doi:10.1021/acs.jpcc.7b12418

37. Benjaram, M. Reddy, Lakshmi Katta, and Gode Thrimurthulu, Novel Nanocrystalline Ce1-xLaxO2-δ (x = 0.2) Solid Solutions: Structural Characteristics and Catalytic Performance, Chem. Mater. 2010, 22, 467–475